Journal of Applied Polymer Science

Preparation and characterization of hyperbranched polymer modified montmorillonite/chlorinated butyl rubber damping composites

Cao Fuhai, Wang Jincheng
Department of Polymer Materials and Engineering, College of Chemistry and Chemical Engineering, Shanghai University of Engineering Science, Shanghai 201620, People's Republic of China
Correspondence to: W. Jincheng (E-mail: wjc406@126.com)

ABSTRACT: In this work, Na^+-montmorillonite (MMT) was modified by hyperbranched polymer (HBP) and grafted with hindered phenol to improve the damping and other properties of the chlorinated butyl rubber (CIIR) composites. The hyperbranched polymer-modified montmorillonite (HBP-OMMT) was prepared by organic montmorillonite (OMMT) that was obtained from the cation exchange reaction between MMT and silane quaternary ammonium salt. The main characterization methods were Fourier transform infrared spectroscopy, hydrogen nuclear magnetic resonance, X-ray diffraction, scanning electron microscopy, energy dispersive spectrometer, and thermogravimetric (TG) analysis. The basal spacings of MMT, OMMT, and HBP-OMMT were 1.47, 2.94, and 4.09 nm, respectively. The onset and center temperatures of decomposition ($T_{-5\%}$ and T_{max}) of HBP-OMMT were improved from 301 and 369 °C to 332 and 398 °C, respectively. The CIIR damping composites were prepared by mechanical blending of HBP-OMMT with pure CIIR. The tensile strength and elongation at break of the composites were improved from 5.4 MPa and 890% to 7.6 MPa and 1066%. From TG curves, $T_{-5\%}$ and T_{max} were increased from 297.4 and 406.0 °C to 323.3 and 410.5 °C, respectively. The dynamic mechanical analysis results showed that tan δ rose from the original 1.20 to 1.44 with the addition of HBP-OMMT. © 2016 Wiley Periodicals, Inc. J. Appl. Polym. Sci. **2016**, *133*, 43645.

KEYWORDS: chlorinated butyl rubber; clay; composites; damping property; hyperbranched polymers

Received 13 June 2015; accepted 11 March 2016
DOI: 10.1002/app.43645

INTRODUCTION

Damping materials had attracted considerable attention both in academia and in industry due to their outstanding properties for reducing vibration and noise in the aerospace, naval vessels, transportation vehicles, and high buildings, and so forth.[1]

Butyl rubber, a kind of copolymer of isobutylene and isoprene, could be divided into both nonhalogenation and halogenation butyl rubber, such as chlorinated butyl rubber (CIIR). CIIR was well known for the higher energy absorptivity and lower molecular mobility compared with other polymers.[2] CIIR showed a unique relaxation behavior: tan δ curve of CIIR revealed an asymmetrical double-peak structure with a maximum on the high-temperature side and an additional shoulder on the other side. However, the loss peak of CIIR occurred at relatively lower temperature region, and it nearly lost the valid damping function in the vicinity of ambient temperatures.[3]

The damping property was extremely related to the morphology of multiphase systems, which included various blends and filling materials.[4] Various fillers could be used to improve the damping properties of polymeric materials. For example, a carbon black transient network was the dominant factor governing the damping property in cured natural rubber.[5] The damping performance of piezoelectric ceramic/CIIR composites was researched. The result showed the maximum tan δ of the composites was 1.05, and the glass transition temperature, T_g, was −31.86 °C. This showed that the effect of modification was not ideal.[6] Nanographite-reinforced chlorobutyl elastomer (CIIR) nanocomposites had also been studied. Results showed that the tensile strength, hardness, and modulus were increased and the elongation at break was decreased with the loading of nanographite. This was attributed to better interactions between CIIR and nanographite. The T_g value was in the range of −10 to 10 °C, and the damping temperature range was obviously improved. However, the damping performance had not been greatly improved.[7] In addition, the layered structure of montmorillonite (MMT) was advantageous to increase the interaction between macromolecular chains, and thus can improve the damping performance of polymers. Wu *et al.* used solution intercalation method to prepare CIIR/MMT composites.[8] Results revealed that the addition of MMT could improve the

damping properties of rubber composites and heighten their thermal decomposition temperatures. Mechanical tests showed that the tensile and impact strength of these composites were significantly improved by incorporation of MMT.[9,10] Moreover, considerable research had been carried out to enhance the damping property of polymeric materials by introducing small molecules, which was widely recognized that the H-bond played a crucial role both in stabilizing static structures and in mediating dynamic performances.[11] Su *et al.* prepared a series of CIIR/acrylate rubber (AR) composites containing oligo-phenol [produced by reacting of 4-methyl-phenol with dicyclopentadiene and isobutylene (MPDI)] as organic fillers. Results showed that MPDI could form hydrogen bonds with AR more easily than with CIIR.[12] Wu *et al.* introduced the hindered phenol of AO-80 into natural rubber matrices. Results demonstrated that the damping property of these composites was effectively improved.[13]

However, till now, the research on the combination of above fillers and small molecules and its application in rubbers had not been conducted. Hyperbranched polymers (HBPs) had highly branched structure and a large number of end groups. In addition, they possessed high reactivity, good solubility, low viscosity, and other properties, especially in the process of synthesis.[14] It is feasible to use this polymer to combine above fillers and small molecules and expected to have novel application properties.

In this article, MMT was first modified by HBP, and then grafted with hindered phenol. This damping agent was applied in CIIR composites. The mechanical properties such as tensile strength, elongation at break, damping, and thermal stability were researched and compared.

EXPERIMENTAL

Materials

Na^+-montmorillonite (SMP, cation exchange capacity = 60–70 mmol/g, denoted as MMT), industrial grade, was obtained from Zhejiang Fenghong Clay Company. The shape was a sheet-like structure, and the interlayer spacing was about 1.5 nm. CIIR (industrial grade 1068), was obtained from Shanghai Zhenghua Industrial. 3-Chloropropyl)methyldiethoxysilane was supplied by Shanghai Guoyao Chemical Company (Shanghai, China). The chemical formula was expressed as

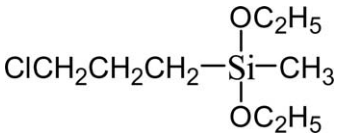

Diisopropanolamine, chemical pure (AR), was supplied by Energy Chemical Company (Shanghai, China). The chemical formula was expressed as

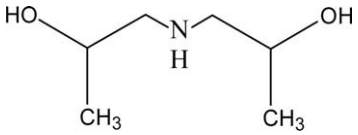

Antioxidant 245, industrial grade (GR), was supplied by Shanghai Anhui Chemical (Shanghai, China). The chemical formula was expressed as

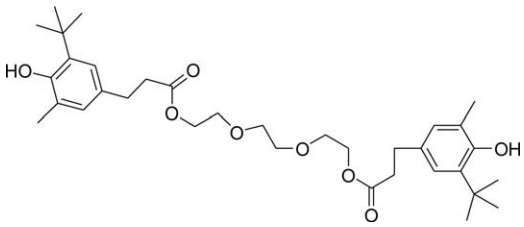

Phthalic anhydride (AR), was supplied by Maya Reagent Company (Shanghai, China). C16-18-alkyldimethylamine (GR), was supplied by Shandong Dingxin Chemical (Shandong, China). Xylene, sodium iodide, anhydrous ethanol, and chloroform were supplied by Shanghai Guoyao Chemical Company (Shanghai, China).

Preparation of Silane Quaternary Ammonium Salt. The anhydrous ethanol solution of (3-chloropropyl)methyldiethoxysilane (30 mL), C16-18-alkyldimethylamine (30 mL), and sodium iodide (0.03 g) were added into the reactor and stirred at 100 °C for 30 h. The product was a kind of pale yellow viscous liquid. Rotary evaporation and distillation method were used to remove the solvent, and then the final product was obtained.

Preparation of Organic Montmorillonite. About 300 mL of de-ionized water and 50 g of MMT were added into a three-necked flask, and vigorously stirred at 60 °C for 5 h. Then, the organic montmorillonite (OMMT) was prepared by the reaction of the priorly prepared silane quaternary ammonium salt and the water treated MMT.[15]

Preparation of AB2 Monomer. About 45 g of phthalic anhydride was gradually added to the chloroform solvent of diisopropanolamine (38 g) in a three-necked flask provided with a stirrer to prepare the AB2 monomer. "A" was the representative of phthalic anhydride, and "B" was the representative of diisopropanolamine.[16]

Preparation of Hindered Phenol. The hindered phenol was obtained by the hydrolysis reaction of antioxidant 245 in NaOH solution at 65 °C for 5 h. The hindered phenol was obtained after acidification, filtration, and drying.

Preparation of HBP-OMMT. The OMMT and AB2 monomer were added into a three-necked flask provided with a stirrer. The mixture was treated at 50 °C for about 1 h. Then, the temperature was increased to 150 °C and stirred for 5 h.The priorly prepared hindered phenol as the blocking agent was added, and then the HBP-OMMT was obtained after purification and drying.

Preparation of CIIR/HBP-OMMT Composites. Different rubber additives together with HBP-OMMT were added into the CIIR systems on a double roller plasticator (Shanghai Second Rubber Machinery Factory, XK-1600, Shanghai, China). The mixture was then mixed for 20 min, and CIIR/HBP-OMMT

Table I. Formulation of CIIR Vulcanizates

Component	Phr (parts per hundred of rubber)
CIIR	100
Zinc oxide	5
Tetramethyl thiuram disulfide	1
Stearic acid	2
N-Phenyl-β-naphthylamine	1
Diben zothiazole disulfide	1
Sulfur	2
HBP-OMMT	0, 5, 10, 15, 20

composites were prepared. Curing was conducted at 170 °C for 30 min, after which an elastic vulcanizate was obtained. The formulation shown in Table I was used for the application of HBP-OMMT. In this description, pure CIIR was denoted as CIIR-0, the CIIR added with 5 phr of damping agent was denoted as CIIR-5, and the rest were denoted as CIIR-10, CIIR-15, and CIIR-20, respectively.

Characterization

Fourier transform infrared (FTIR) spectra were obtained using a spectrometer, model Avatar 370 from Nicolet Corporation. The scanning range was from 4000 to 650 cm^{-1} with a resolution of 2 cm^{-1}.

Hydrogen nuclear magnetic resonance (^{1}H-NMR) (BrukerAV600 spectrometer) was used to analyze the components of the silane quaternary ammonium salt and AB2 monomer.

Scanning electron microsco (SEM) was observed using a Hitachi S-2150 SEM. The SEM was taken using an electron beam potential of 25 kV. Energy dispersive spectrometer (EDS) was the genesis type spectrum analyzer from EDAX Company of the United States. The EDS was used for the composition analysis according to different elements characteristic energy of X-ray photons. The EDS was applied to analyze the content of each element in the MMT, OMMT and HBP-OMMT.

TG analysis was carried out at 20 °C/min heating rate from ambient temperature to 600 °C in nitrogen atmosphere. This was conducted by a Linseis PT-1000 microbalance and was controlled by Version 3.0 software. In each case, the mass of the samples used was fixed at 10 mg.

X-ray diffraction (XRD) was performed at ambient temperature with a Rigaku D-Max/400 X-ray diffractometer (Japan). The X-ray beam was nickel filtered CuKα ($\lambda = 0.154$ nm) radiation and was operated at 50 kV and 70 mA. The diffraction data were obtained from 1 to 10° (2θ) at a rate of 2°/min.

The tensile properties of CIIR composites were measured with dumbbell specimens (6 mm wide in cross section) according to the Chinese National Standard GB 528-82. The tests were carried out at room temperature on a universal tensile testing machine (TCS-2000, Dongguan, China) with a cross-head speed of 500 mm/min.

Dynamic mechanical analysis (DMA) was carried out using a USA Q800 instrument. This test was conducted from −70 to 50 °C with a heating rate of 3 °C/min at liquid nitrogen condition. The damping factor, storage modulus, and loss modulus of the samples were measured.

RESULTS AND DISCUSSION

The Analysis of Silane Quaternary Ammonium Salt. "Nucleophilic substitution" reaction occurred between the (3-chloropropyl)methyldiethoxysilane and C16-18-alkyldimethylamine under the action of the catalyst, sodium iodide. The characteristic absorption peaks of C16-18-alkyl dimethylamine at 2920, 2850, and 1460 cm^{-1} were caused by C—H stretching, and the absorption peak at 1040 cm^{-1} was related to C-N bond [Figure 1(a)]. The peaks at 950, 862, and 789 cm^{-1} of (3-chloropropyl) methyldiethoxysilane [Figure 1(b)] were probably assigned to the stretching vibration of Si—O—C bond and the bending vibration of Si—C bond. The strong absorption band at 1060 cm^{-1} was resulted from the stretching vibration of Si—O.[17] The peaks at 2800–3000 and 1440 cm^{-1} of silane quaternary ammonium salt [Figure 1(c)] were caused by C—H stretching. The successful nucleophilic substitution reaction between (3-chloropropyl) methyldiethoxysilane and tertiary amine was obtained from the increased intensity of peaks.[18] A new peak appearing at 914 cm^{-1} was resulted from corresponding stretching absorptions of N—Cl in the monomer. The significantly enhanced absorption band at 1470 cm^{-1} was attributed to flexural vibrations of —CH_3 in the cation —$(CH_3)_2N^+(CH_3)_2N$.[19] This illustrated that the successful nucleophilic substitution reaction occurred between the components [Scheme 1(a)].

In Figure 2(a), the ^{1}H-NMR of C16-18-alkyldimethylamine, the chemical shifts at 1–3 ppm may be due to the hydrogen in C-H bonds. The chemical shifts at 0.1–0.2, 0.8–0.9, and 1.2–1.5 ppm of silane quaternary ammonium salt [Figure 2(b)] were resulted from the structure of —CH_2—$Si(CH_3)(OCH_2$—$CH_3)_2$, which appeared in both of the two materials. The band at 1.8 ppm may be attributed to the structure of $(CH_3)_2NCH_2Cl$ and disappeared in the spectrum of silane quaternary ammonium salt [Figure 2(c)]. Moreover, new bands appeared between 2.3 and 2.4 ppm, which may be attributed to the structure,

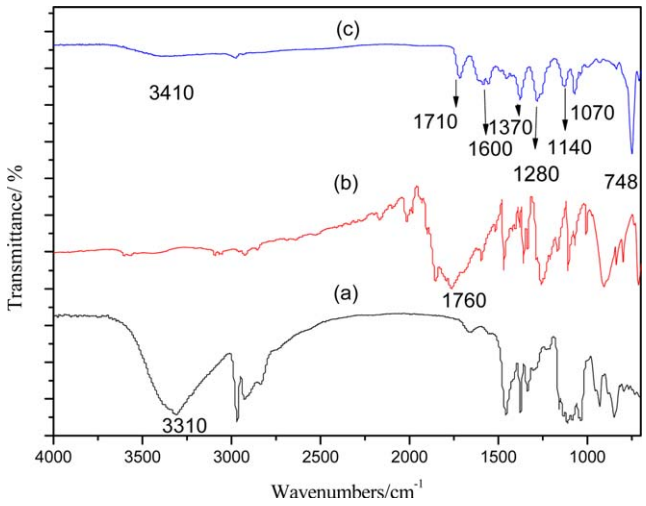

Figure 1. FTIR of (a) C16-18-alkyldimethylamine, (b) (3-chloropropyl)methyldietho-xysilane, and (c) silane quaternary ammonium salt. [Color figure can be viewed in the online issue, which is available at wileyonlinelibrary.com.]

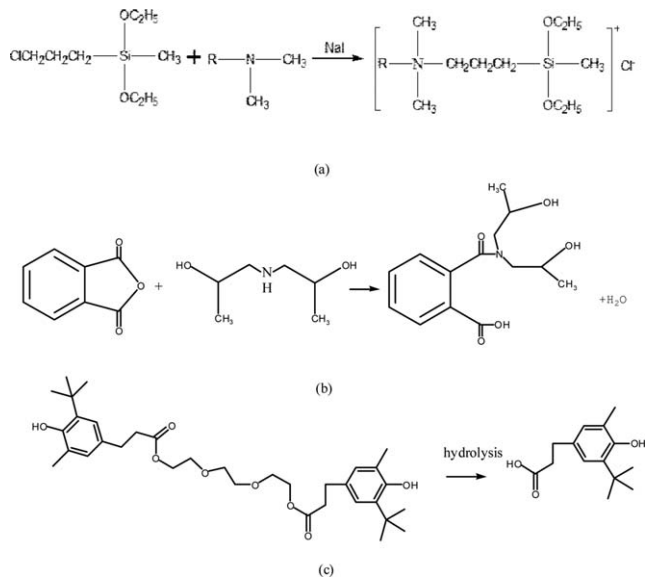

Scheme 1. Chemical formula for preparation of (a) silane quaternary ammonium salt, (b) AB2 monomer, (c) hindered phenol.

CH_3—$N^+(CH_2)_2$-. This was ascribed to the dimensional structure of monomers and the high electronegativity of nitrogen atom.[20] In summary, above analysis together with FTIR demonstrated that the silane quaternary ammonium salt was successfully synthesized.

The Analysis of AB2 Monomer. The synthesis of AB2 monomer was conducted by the way of dehydration condensation reaction between phthalic anhydride and diisopropanolamine. The structural formula was shown in the Scheme 1(b). The peak at 3210–3550 cm^{-1} was stretching vibration of —NH— and —OH in diisopropanolamine [Figure 3(a)]. The absorption bands at 1750–2000 cm^{-1} were stretching vibration of the anhydride group in phthalic anhydride [Figure 3(b)]. The above two groups disappeared in the spectrum of AB2 monomer [Figure 3(c)]. Hereby, two absorption peaks appeared at 1560–1610 cm^{-1} (ν C═O in amide groups) and 1710 cm^{-1} (ν C═O in ester groups). The bands 1070 cm^{-1} was attributed to and C—N stretching, and the bands 1140, 1280, and 1370 cm^{-1} may be due to the C—O stretching. This indicated the reaction occurred between the secondary amine in diisopropanolamine and the anhydride group in phthalic anhydride was successful, and thus amide and carboxyl groups were produced. Amin *et al.*[21] used the bulk reaction of diisopropanolamine and phthalic anhydride to prepare the HBP. Characteristic absorption peaks appeared at 1623–1612 cm^{-1} (ν C═O in amide groups), 1721–1720 cm^{-1} (ν C═O in ester groups), 1276–1269 cm^{-1} (ν C—O), and 1065–1064 cm^{-1} (ν C—N). This HBP showed different absorption peaks compared with what the work synthesized. This may be ascribed to the different polymerization methods and reaction conditions. High reaction temperatures were required in their experiment due to the difficulty of controlling the reactions to obtain the desired polymer. However, solution polymerization was used in our experiment to prepare the HBP. In this experiment, low molecular weight of HBP was needed due to its requirement to intercalate MMT. This reaction was easy to be controlled and the low temperature was used. The condensation reaction occurred and converted the carboxyl groups to ester in an esterification reaction. The bands from 1276–1269 to 1065–1064 cm^{-1} were attributed to C—O and C—N stretchings.[22] In addition, the absorptions at 3200–3600 cm^{-1} were stretching vibration of —OH. Moreover, the peaks at 748 cm^{-1} were a result of the stretching vibration of the benzene ring. The intensity of absorption peak at 1700 cm^{-1} became weaker compared with that of the phthalic anhydride. This may be due to the reaction between anhydride and ester groups. To sum up, the successful addition reaction between diisopropanolamine and phthalic anhydride was demonstrated.

The bands appearing between 7.5 and 8.5 ppm of phthalic anhydride [Figure 4(b)] were attributed to the structure of benzene ring.[21] The chemical shifts at 2–3 ppm were resulted from —NH— in diisopropanolamine [Figure 4(a)], which disappeared in the spectrum of AB2 monomer [Figure 4(c)]. The signal at 3.8 ppm may be due to the proton of hydroxyl group, while the signals at 1–2 ppm were assigned to the proton in C-H bond. This result illustrated that all diisopropanolamine had been

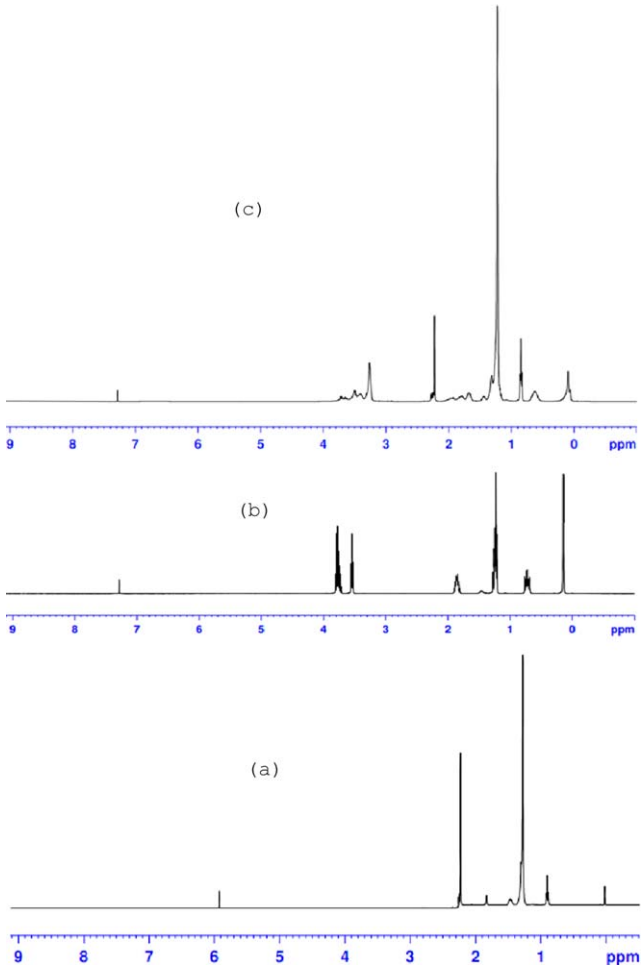

Figure 2. ^{1}H-NMR of (a) C16-18-alkyldimethylamine, (b) (3-chloropropyl)methyldiethoxysilane, and (c) silane quaternary ammonium salt. [Color figure can be viewed in the online issue, which is available at wileyonlinelibrary.com.]

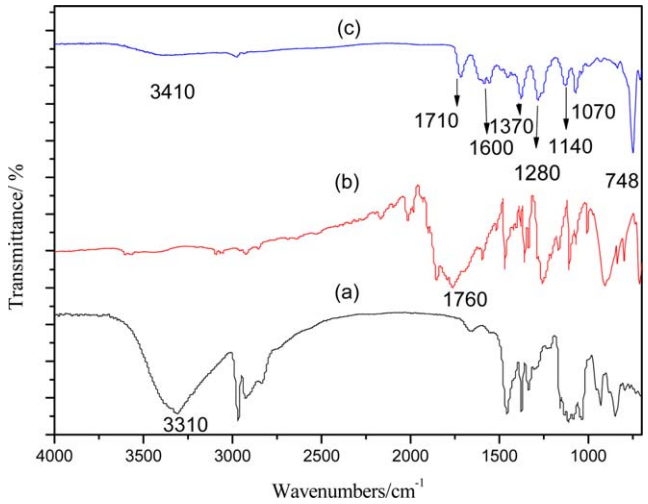

Figure 3. FTIR of (a) diisopropanolamine, (b) phthalic anhydride, and (c) AB2 monomer. [Color figure can be viewed in the online issue, which is available at wileyonlinelibrary.com.]

reacted in the system together with the successful preparation of AB2 monomer. Amin *et al.*[21] obtained the similar results in the ^{1}H-NMR curves of their HBP. The chemical shifts at 2.97–3.38 ppm were assigned to O═CN—CH_2, and the shifts at 4.48 ppm was resulted from —OH. Compared with the chemical shifts of the HBP we synthesized, the small deviation may be due to their difference in polymerization method and molecular weight.

The Analysis of Hindered Phenol. The characteristic absorption peaks of the antioxidant 245 [Figure 5(a)] were shown at 1740 and 1080–1140 cm^{-1}, which were caused by the stretching vibration of —COO and C—O—C. Stronger peaks of hindered phenol [Figure 5(b)] appeared around 3600 and 1500 cm^{-1}. This illustrated that more —OH groups may exist in this compound and the successful hydrolyzation of the antioxidant was demonstrated.

The chemical shifts at 5.1 and 7.0–7.5 ppm were resulted from Ph—OH and Ph—H, while 1.3–1.6 and 2.5–3.0 ppm may come from Ph—CH_2—CH_2— groups. The chemical shifts of antioxidant 245 [Figure 6(a)] between 3.5 and 4.5 ppm were ascribed to —CH_2—O— groups. In addition, the chemical shifts were not found in the spectrum [Figure 6(b)], and such changes were the evidence of the successful reaction [Scheme 1(c)].

The Analysis of OMMT and HBP-OMMT. OMMT was prepared by cation exchange reaction between MMT and the silane quaternary ammonium salt (Scheme 2). HBP-OMMT was obtained by condensation polymerization between OMMT, AB2 monomer, and the hindered phenol. Hydroxyl groups that produced by hydrolysis of silane quaternary ammonium salt were reacted with the carboxyl group of AB2 monomers to prepare HBP (Scheme 3).

FTIR Analysis. FTIR spectrum of the characteristic absorption peak of MMT [Figure 7(a)] at 1010 cm^{-1} was attributed to stretching and bending absorptions of Si—O and Al—O in the inorganic silicate layers. The bands at 3435 and 1635 cm^{-1} were results of the structural -OH groups in MMT. The new peaks at 2800–3000 and 1460 cm^{-1} in the spectrum of OMMT [Figure 7(b)] were caused by C-H stretching. Moreover, the absorptions at 3200–3600 cm^{-1} were a result of —OH stretching vibration in Si—OH structure.[23] New peaks at 1710 cm^{-1} of HBP-OMMT [Figure 7(c)] were attributed to —C═O and —C—O bonds in the HBP. In addition, the peaks at 1070, 789, and 744 cm^{-1} were typical for stretching vibrations of Si—O, Al—O, and benzene ring bonds in HBP-OMMT structure.[24] The OMMT had a vibration at 1640 cm^{-1} and this was the bending vibrations for the adsorbed water together with the hydroxyl groups in silane quaternary ammonium salt.[17] However, the FTIR absorption bands in the low-frequency region of MMT, OMMT, and HBP-OMMT exhibited different intensity peaks at about 1000 cm^{-1}. This indicated the structure and composition of clay mineral had changed upon exchange of the interlayer

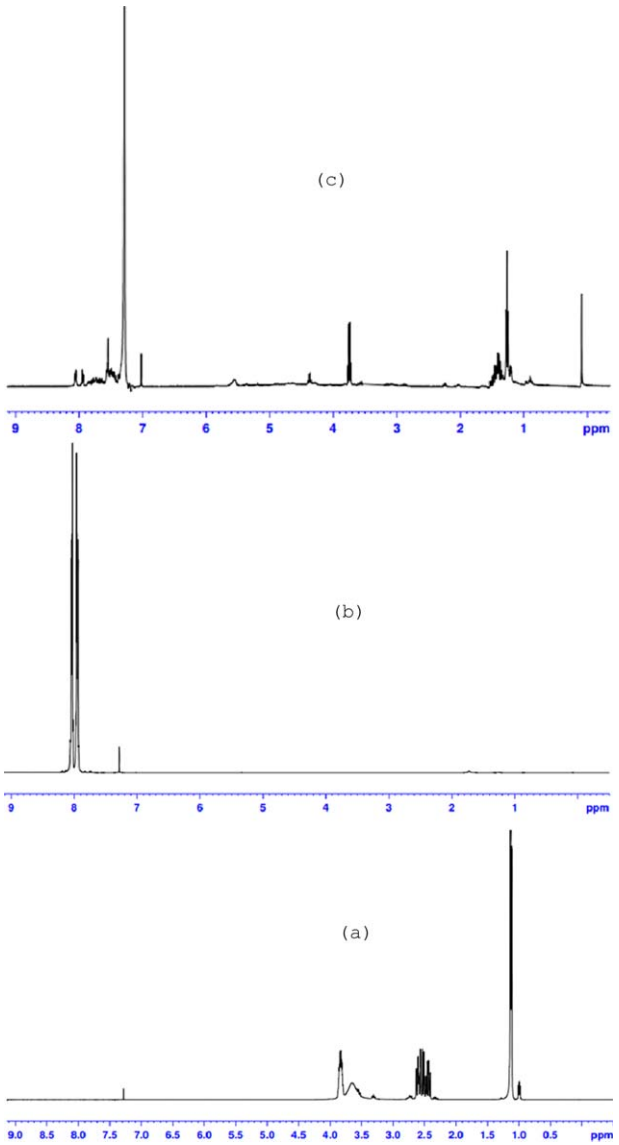

Figure 4. ^{1}H-NMR of (a) diisopropanolamine, (b) phthalic anhydride, and (c) AB2 monomer. [Color figure can be viewed in the online issue, which is available at wileyonlinelibrary.com.]

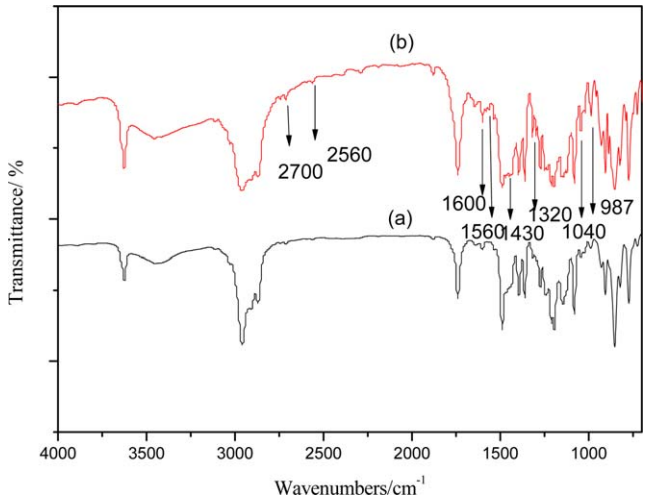

Figure 5. FTIR of (a) antioxidant 245 and (b) hindered phenol. [Color figure can be viewed in the online issue, which is available at wileyonlinelibrary.com.]

sodium ions by the quaternary ammonium salts and HBP. Some of quaternary ammonium salts and HBP could pass through a portion of the layer of MMT, and thus exfoliated the layered structure.[25] The successful preparation of OMMT and HBP-OMMT can be preliminarily demonstrated by above analysis.

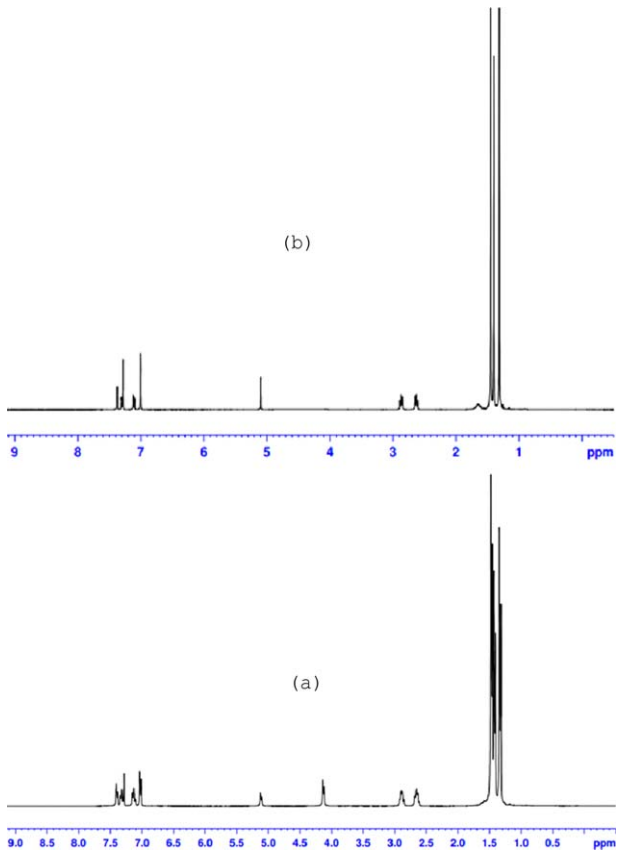

Figure 6. [1]H-NMR of (a) antioxidant 245 and (b) hindered phenol. [Color figure can be viewed in the online issue, which is available at wileyonlinelibrary.com.]

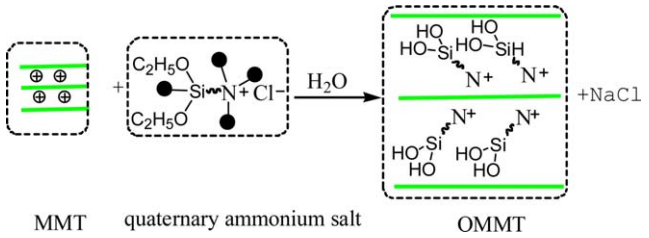

Scheme 2. Preparation process of OMMT. [Color figure can be viewed in the online issue, which is available at wileyonlinelibrary.com.]

XRD Analysis. XRD curves of MMT, OMMT, and HBP-OMMT were shown in Figure 8. The data were obtained by calculating from Bragg formula: $2d \sin\theta = n\lambda$. The reflection was shown at 6.0° [Figure 8(a)], and the basal interlayer spacing was 1.47 nm for MMT. As for OMMT [Figure 8(b)], the appreciably larger basal spacing (2.94 nm) for OMMT may be due to the oblique-parallel arrangement of quaternary ammonium salts during synthesis.[17,26] The basal spacing of HBP-OMMT [Figure 8(c)] was 4.09 nm, and this was larger than that of MMT and OMMT. This may be ascribed to disorderedly expanded state of HBP during synthesis. Only one peak appeared in the curves of OMMT and HBP-OMMT. This implied that the molecules were uniformly present in the interlayer space of the silicate layers, which illustrated a good intercalation effect presented in these organoclays. From Figure 8(b,c), some of the basal reflection

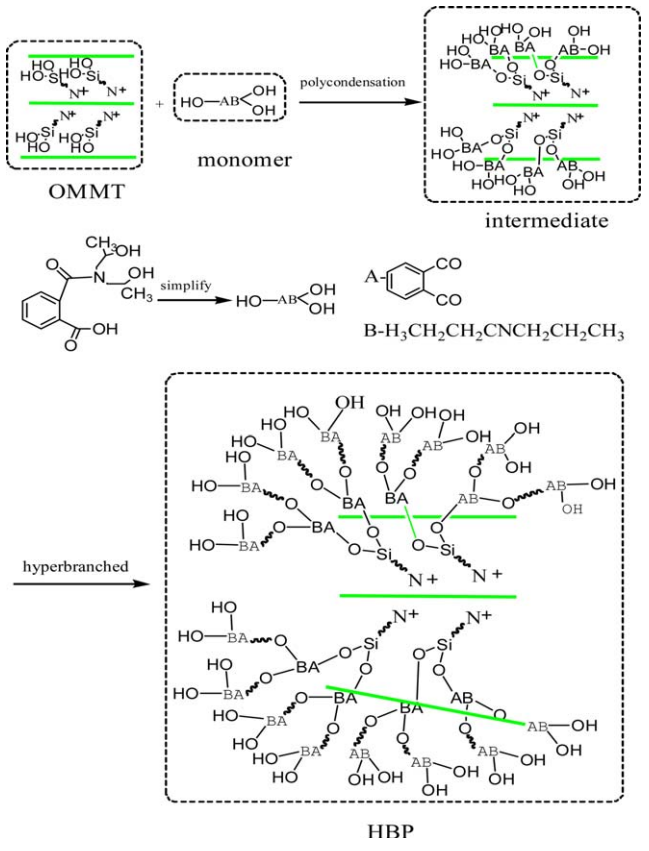

Scheme 3. Preparation process of HBP-OMMT. [Color figure can be viewed in the online issue, which is available at wileyonlinelibrary.com.]

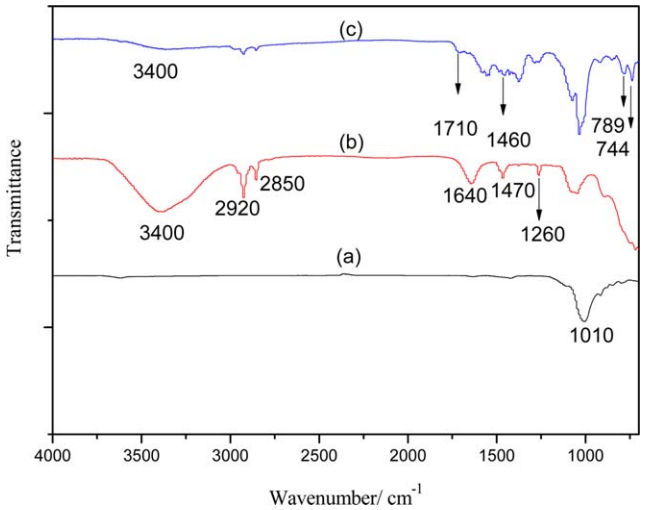

Figure 7. FTIR of (a) MMT, (b) OMMT, and (c) HBP-OMMT. [Color figure can be viewed in the online issue, which is available at wileyonlinelibrary.com.]

cannot be detected from the peaks of OMMT and HBP-OMMT. The intercalation of HBP macromolecules into MMT could expand the interlayer space from 1.47 to 4.09 nm, and even to exfoliation. The formation of a larger interlayer spacing may be ascribed to the arrangement of the HBP molecules together with the enhanced interactions between molecules and the silicate layers. In addition to the experimental evidence, Piscitelli *et al.* revealed that larger value of estimated basal spacing was obtained upon increasing the number of molecules within the MMT interlayer spaces due to the weakening attracted forces among the layers.[27] The unusually wide interlayer space was directly related to the sprawl structure of the HBP segment. [28] Moreover, the functional groups in the exterior of HBP could greatly influence the intercalation profile in the layered confinement.[29] On the basis of above information, the quaternary ammonium salts and HBP could be encapsulated in the interlayer spaces as conceptually described in Scheme 3.

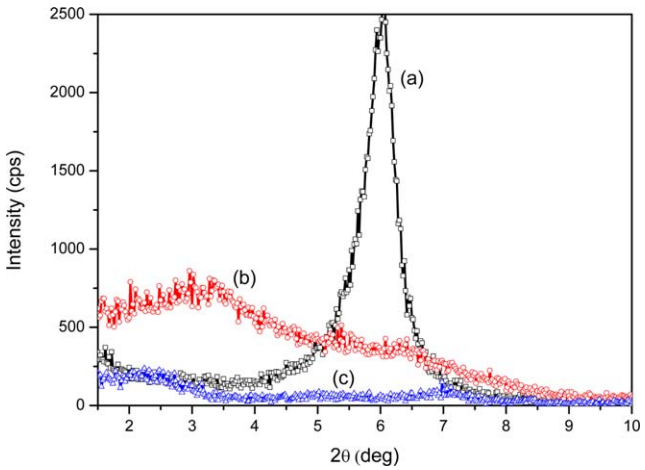

Figure 8. XRD of (a) MMT, (b) OMMT, and (c) HBP-OMMT. [Color figure can be viewed in the online issue, which is available at wileyonlinelibrary.com.]

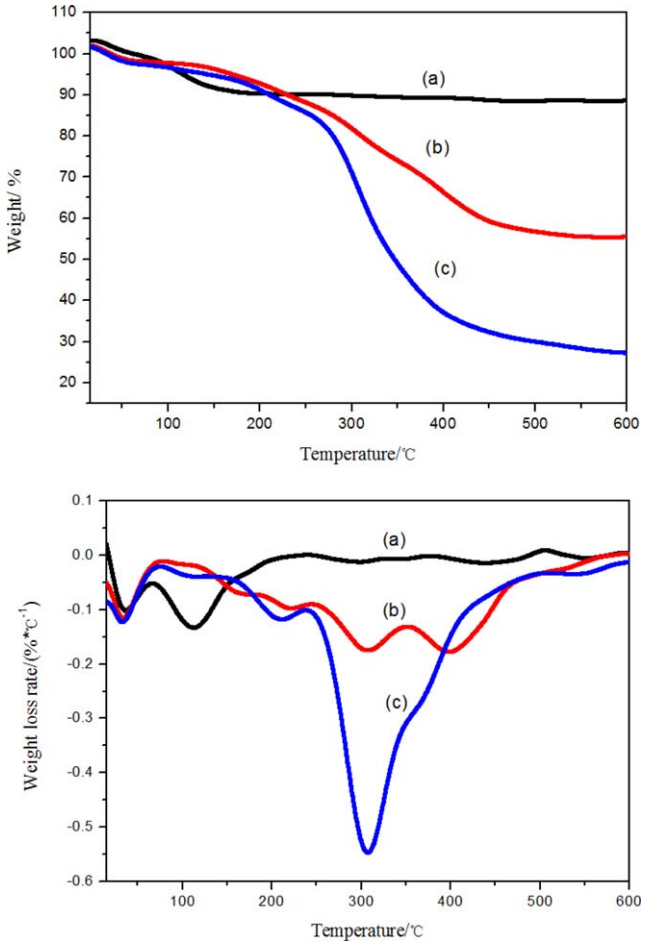

Figure 9. TG and DTG of (a) MMT, (b) OMMT, and (c) HBP-OMMT. [Color figure can be viewed in the online issue, which is available at wileyonlinelibrary.com.]

TG Analysis. The thermal stability of MMT [Figure 9(a)] under nitrogen consisted of two main stages. In the first stage, the free water molecules physically adsorbed on the external surfaces and the hydrating water molecules inside the interlayer space were removed due to the improvement of temperatures from ambient to 200 °C. The second stage was attributed to the dehydroxylation of the structural silanol units of the MMT in the range of 200–600 °C.[30] Dehydration order depended on the formation process of the adsorbed water and the interaction strength.[31] The OMMT [Figure 9(b)] and HBP-OMMT [Figure 9(c)] undergone a four-step decomposition process. The vaporization of free water occurred at temperatures below 200 °C, and the decomposition of surfactant taken place between 200 and 500 °C. The weight losses of the modified MMTs between 200 and 500 °C were due to the decomposition of the organics over the surfaces of the silicate layers. The decomposition products of OMMT were probably carbonaceous residues including the carbon chain framework and the silicon carbon residues.[23] The weight losses of HBP-OMMT between 200 and 500 °C may be due to the decomposition of HBP and the organic salts. In addition, around 300 °C, the weight losses of HBP-OMMT were significantly more than that of OMMT. This showed that more organic compound existed in HBP-OMMT and illustrated the

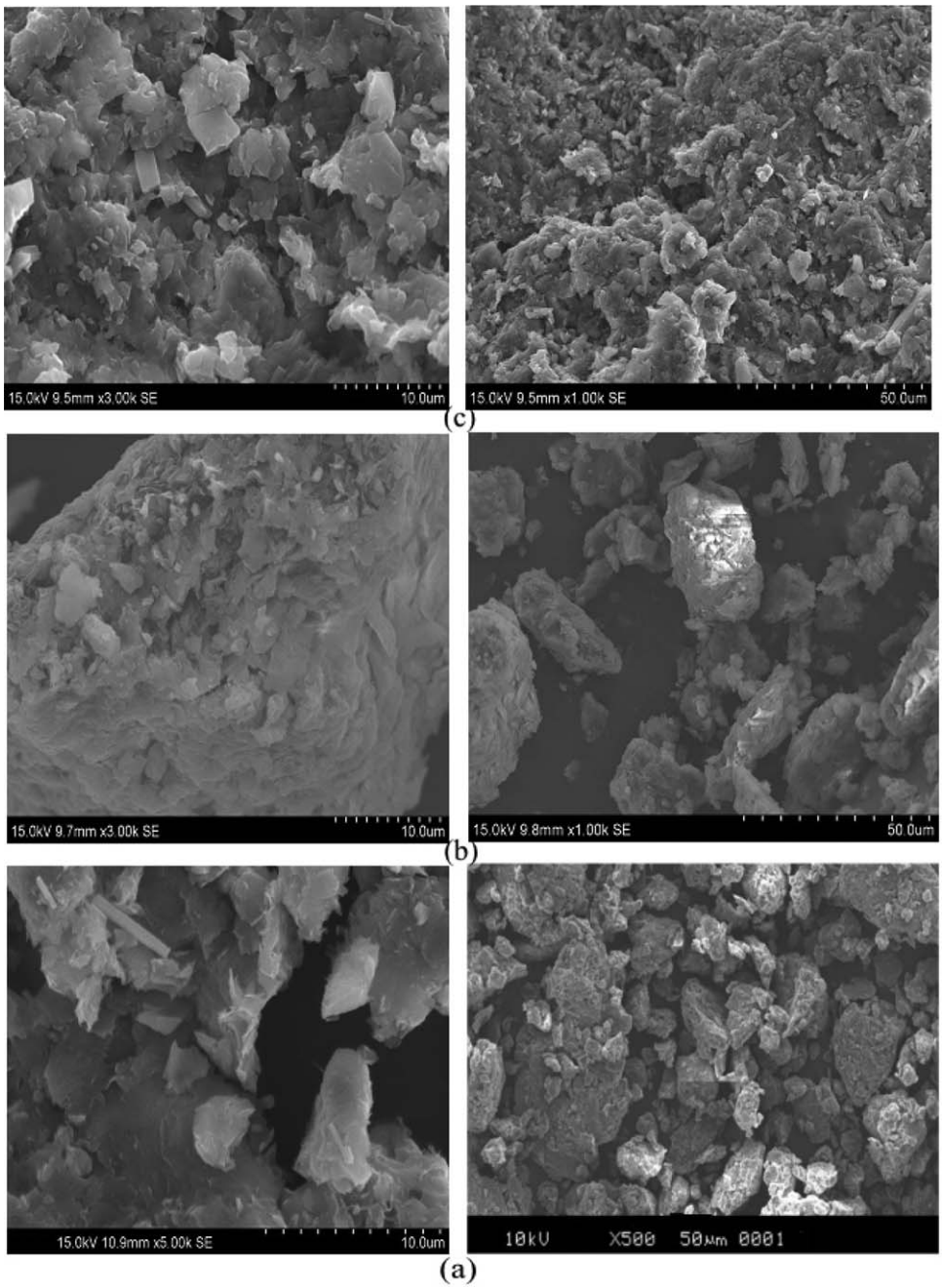

Figure 10. SEM of (a) MMT, (b) OMMT, and (c) HBP-OMMT.

Table II. EDS Data of MMT, OMMT, and HBP-OMMT

	MMT		OMMT		HBP-OMMT	
Element	wt %	At %	wt %	At %	wt %	At %
C	0	0	43.10	58.78	75.28	83.06
Na	3.35	3.15	1.05	0.71	0.35	0.19
O	31.74	45.29	19.62	20.09	15.33	12.70
Si	44.37	36.06	24.01	14.01	5.91	2.79

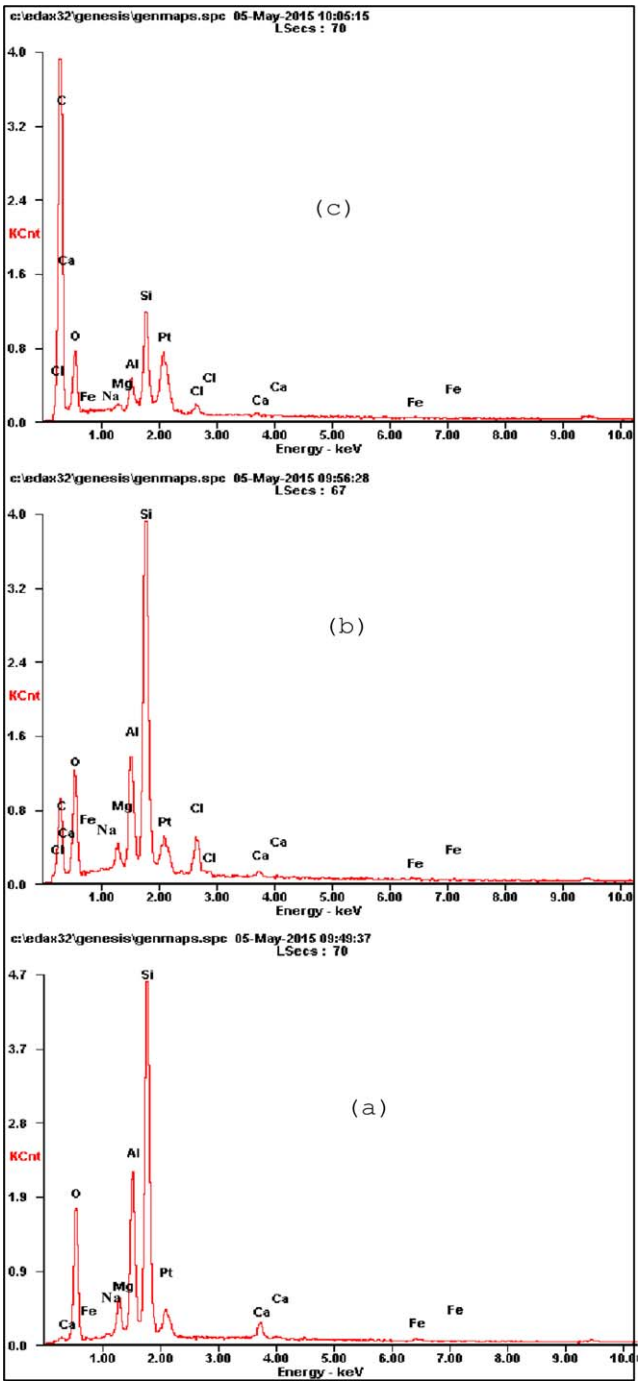

Figure 11. EDS of (a) MMT, (b) OMMT, and (c) HBP-OMMT. [Color figure can be viewed in the online issue, which is available at wileyonlinelibrary.com.]

initial formation of residual carbonaceous product.[32] Dehydroxylation of the MMT layers occurred after 500 °C. The last step was the decomposition associated with the combustion reaction between organic carbon and inorganic oxygen.[30,33]

SEM and EDS Analysis. SEM was used to observe the microstructure and morphology of MMT, OMMT, and HBP-OMMT (Figure 10). MMT was formed by large powders with lower surfactant packing density [Figure 10(a)]. It was mainly composed of regular layers stacking with a number of curved mineral layers. OMMT was modified by the quaternary ammonium salts, and some small powders could be found [Figure 10(b)]. This meant that the surface structure of OMMT was changed and possessed partial exfoliated phenomenon.[34] However, lots of large particles were still found in the OMMT, which may be due to the formation of bonds between the particles which resulted from the indivisible water in the silicate layers. Abreu *et al.* found the same phenomenon in their experiments. After the addition of Ag-NPs to the nanostructure C30B/ST films, the dispersion of Ag-NPs can be contributed to the formation of more exfoliated structure.[35] However, the basic structure of OMMT with regularly arranged lamellars had not been changed. The HBP-OMMT [Figure 10(c)] was composed of small powders, and the largest power was about 5–10 μm. Polymeric materials were covered over the surface of HBP-OMMT. Many small silicate layers were embedded in the large ones, and the regularly arranged lamellar disappeared.[36] This phenomenon indicated that hyperbranched technology was beneficial for the dispersion of these aggregated powders.

EDS was a more precise characterization method for intercalation effect. The EDS results of MMT, OMMT, and HBP-OMMT were shown in Figure 11 and Table II. With the addition of organic molecules, the content of C elements increased considerably in OMMT and HBP-OMMT. Compared with that of MMT which had no carbon element, the weight ratio of carbon in OMMT and HBP-OMMT was increased to 43.10 and 75.28%, respectively. However, the content of Na, O, and Si elements in OMMT and HBP-OMMT had decreased significantly. As for OMMT, the sodium ions were replaced by the quaternary ammonium salts intercalated into the layers of MMT due to the ion exchange reaction. This led to the decreased content of sodium elements. In HBP-OMMT, the amount of polymer was increasing, and this resulted in destroying of the layered structure of organoclay. Moreover, the increased polymer content also reduced the contents of Si, O, and other elements in these silicate layers.

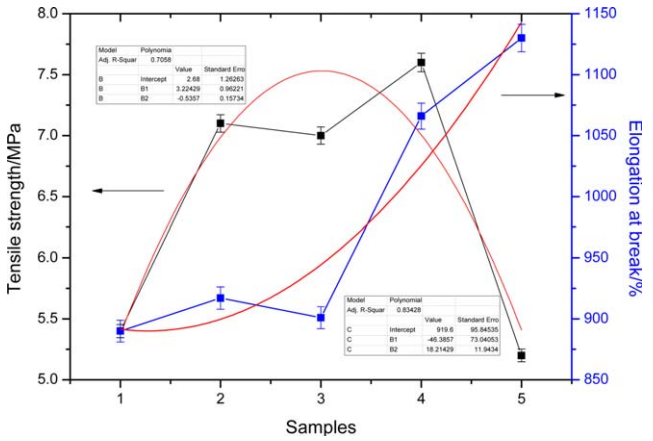

Figure 12. Tensile properties of different CIIR composites (samples, 1-CIIR-0, 2-CIIR-5, 3-CIIR-10, 4-CIIR-15, 5-CIIR-20). [Color figure can be viewed in the online issue, which is available at wileyonlinelibrary.com.]

The Analysis of CIIR/HBP-OMMT Composites.

Tensile Properties. The tensile strength of CIIR-15 (Figure 12) was 7.6 MPa, and was improved 41% compared with that of pure CIIR, 5.4 MPa. The tensile strength of CIIR-5 and CIIR-10 was 7.1 and 7.0 MPa, respectively, which was also improved 31 and 30%. The elongation at break of these composites was gradually rising. The elongation at break of CIIR-15 was 1066%, which was increased 20% compared with that of pure CIIR, 890%. From the trend line of the tensile strength and the amount of damping agent, the tensile strength was first increased and then decreased. In addition, the trend line of the elongation at break was continuously increased. The increase of the tensile properties of above composites was resulted from the complex interplay and the induced increase in the apparent degree of crosslinking between HBP-OMMT and the CIIR segments. HBP had a large number of branches and a large number of highly reactive functional groups in the end. The branches can entangle with the segments of rubber molecular chains, and thus can increase the crosslinking networks in the polymer matrix. Dodiuk-Kenig *et al.* also found the similar phenomenon of crosslinked chains. The hyperbranched components caused higher crosslinking density, and this resulted in higher stiffness of the adhesive.[37] Mo *et al.* found the same segment motion in their experiments. The activated functional groups can react with the rubber activation point, especially CIIR, which contained an activated chlorine.[38] In addition, the end of HBP had lots of hindered phenol groups to form hydrogen bonds with CIIR, and thus can enhance the interaction with the segments. Based on the above, a large number of segments were formed with CIIR segments by HBP motion, and thus the tensile strength was significantly improved. Meanwhile, the segments movement was hindered by the layered structure of organoclays, and this also increased the tensile strength.

When more HBP-OMMT was added, for example, CIIR-20, its tensile strength was decreased due to the worse compatibility in this composite. In HBP-OMMT, the silicate layers of MMT played a reinforcement role in the composites. The silicate layers may be aggregated inside the composite and lots of gaps were formed in the material with the addition of more HBP-OMMT. However, the elongation at break of CIIR-20 was improved compared with that of CIIR-15. This was ascribed to the effect of another component, HBP, in HBP-OMMT. The HBP possessed low crosslink density, good ductility, and some lubricating ability. Thus, the elongation at break of the composites was improved when its amount was increased.

TG Analysis. As illustrated in TG and DTG curves (Figure 13), the thermal stability of CIIR-15 was better than that of pure CIIR and the other samples. To compare their thermal stabilities clearly, three parameters of $T_{-5\%}$ ($T_{-5\%}$, the temperature at which weight loss is 5%), T_{max} (T_{max}, the temperature at which weight loss is the fastest), and the residues were measured (Table III). $T_{-5\%}$ and T_{max} of CIIR-15 were 323.3 and 410.5 °C, which were higher than that of pure CIIR, 297.4 and 406.0 °C. Due to the complicated polymer matrix and the strong interactions among HBP, the decomposition rate of polymer chains was reduced. However, $T_{-5\%}$ of CIIR-5, CIIR-10, and CIIR-20 was lower compared with that of CIIR-0. The reason for this result was probably due to the residual volatile solvent. When 15 phr of the damping agent was added, the composite had a good degree of compatibility and strong interactions between segments. This limited the aforementioned volatile behavior, and thus CIIR-15 had a high $T_{-5\%}$. The higher decomposition temperatures indicated the improved thermal stability of the composites.[39] After adding the damping agent, T_{max} of all the samples was higher than that of CIIR-0. T_{max} of CIIR-10 was the highest, and the residue of CIIR-15 was the most. In a word, considering above results, CIIR-15 was considered to possess the best thermal properties. However, in the composites, the amount of the residue was decreased compared to the initial content of HBP-OMMT. The increase of the amount of damping agent in the composites would change their properties. When the amount of damping agent was too large, the compatibility of the composites may be poor, and the overall performance such as thermal stability was decreased. Thus, the residues of CIIR-20 were decreased significantly.

Dynamic Mechanical Analysis. The damping behavior of HBP-OMMT in the CIIR composites was assessed by DMA (Figure 14). Tan δ of CIIR-0, CIIR/MMT, CIIR/OMMT, CIIR-15, and CIIR-20 samples was 1.20, 1.29, 1.34, 1.44, 1.31 and they appeared at −42, −36, −31, −29, and −31 °C, respectively. Thus, after adding MMT and OMMT, the damping properties had been increased compared with that of pure CIIR. Meanwhile, the damping property of CIIR/OMMT was better that of CIIR/MMT. This may be resulted from the expanded spacing of OMMT. Under external force, the interlayers of OMMT slipped and this consumed much mechanical energy. Thus, the damping performance of CIIR/OMMT was improved. The concentration and intercalation structure of HBP-OMMT had an influence on the dynamic mechanical properties of the CIIR composites. Therefore, with an increase of HBP-OMMT content, tan δ of CIIR-15 and CIIR-20 was higher than that of others composites. In addition, as for CIIR-15 and CIIR-20, the effective damping temperature ranges were much wider than that of CIIR-0. Within the composites, the hyperbranched damping agent and the segment of CIIR could be entangled and crosslinked. These results were in good accordance to the results of XRD and mechanical tests. With an external force, most of segments were driven to move. However, the layered structure of the organoclay can hinder the movement of these chain segments. Based on the above, the interactions between segments as well as the interactions between the organoclay and segment were enhanced.[1] This led to the increase of internal friction. Thus, more mechanical energy was turned into internal energy, and the damping performance was improved. In addition, intramolecular and intermolecular hydrogen bonds were formed and this was resulted from the end groups of the damping agent. When the hydrogen bonds were broken, the mechanical energy was turned into thermal energy. This could also be beneficial for the improvement of the damping properties. However, compared with CIIR-15, the damping properties of CIIR-20 were decreased. This was ascribed to the worse compatibility in this composite. The "sea-island" structure was formed inside the composites, and the complex interactions between segments

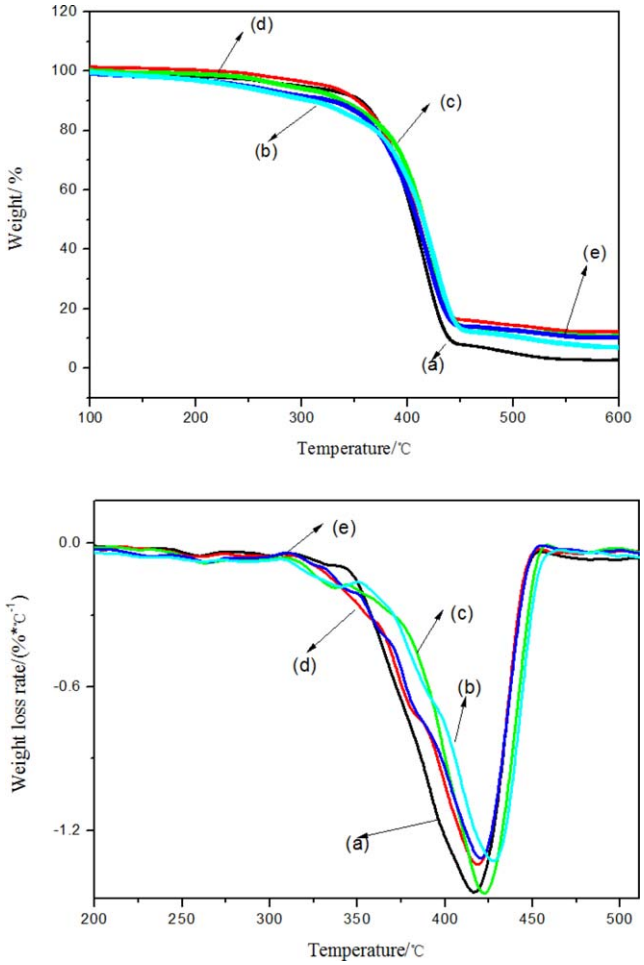

Figure 13. TG and DTG of (a) CIIR-0, (b) CIIR-5, (c) CIIR-10, (d) CIIR-15, and (e) CIIR-20. [Color figure can be viewed in the online issue, which is available at wileyonlinelibrary.com.]

were reduced. This may lead to the decrease of the damping performance.

SEM Analysis. SEM of the fracture surface of CIIR composites was shown in Figure 15. From Figure 15(a), there were a lot of bare small particles presented over the surface of CIIR-0, and the small particles and rubber matrix were separated from each other. In Figure 15(b), the section morphology of CIIR-5 was more flat compared with CIIR-0. There were no large particles in the surface, and the particles were dispersed evenly and wrapped in the rubber matrix. This may be due to a small amount of silicate layers existed in the rubber matrix. From the section morphology of CIIR-10 and 15 [Figure 15 (c,d)], more

Table III. TG Results of Different CIIR Composites

Samples	CIIR-0	CIIR-5	CIIR-10	CIIR-15	CIIR-20
$T_{-5\%}$ (°C)	297.4	250.0	285.0	323.3	239.1
T_{max} (°C)	406.0	408.8	415.4	410.5	414.6
Residue (wt %)	2.7	10.6	10.7	12.3	7.0

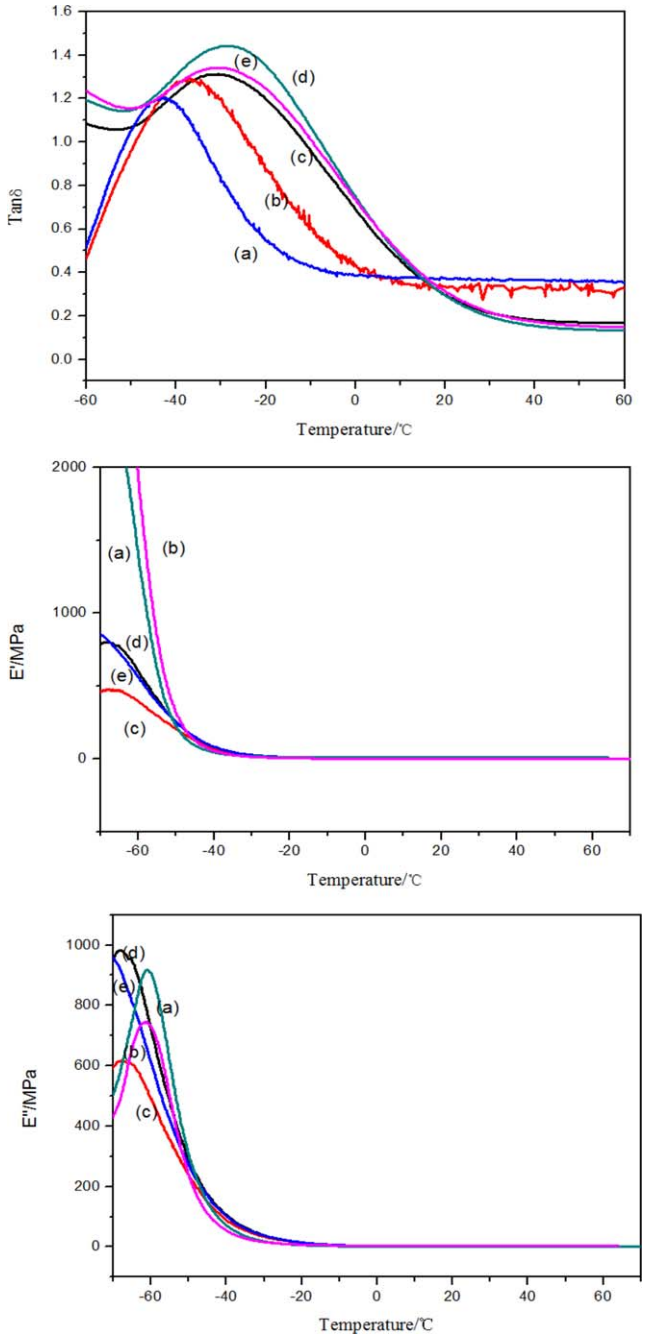

Figure 14. DMA of (a) CIIR-0, (b) CIIR/MMT, (c) CIIR/OMMT, (d) CIIR-15, and (e) CIIR-20. [Color figure can be viewed in the online issue, which is available at wileyonlinelibrary.com.]

and more large particles were found in these sections. Although the compatibility of these composites was a litter decreased, these silicate layers still had a good compatibility with the rubber matrix. Thus, the tensile strength of CIIR-10 and CIIR-15 were improved. With the further increase of the damping agent content, CIIR-20, the compatibility of the composite was getting worse. Lager particles were formed due to the poor dispersion of the silicate layers in the composite, and thus there was a phenomenon of agglomeration. As a result, the tensile strength of CIIR-20 was decreased.

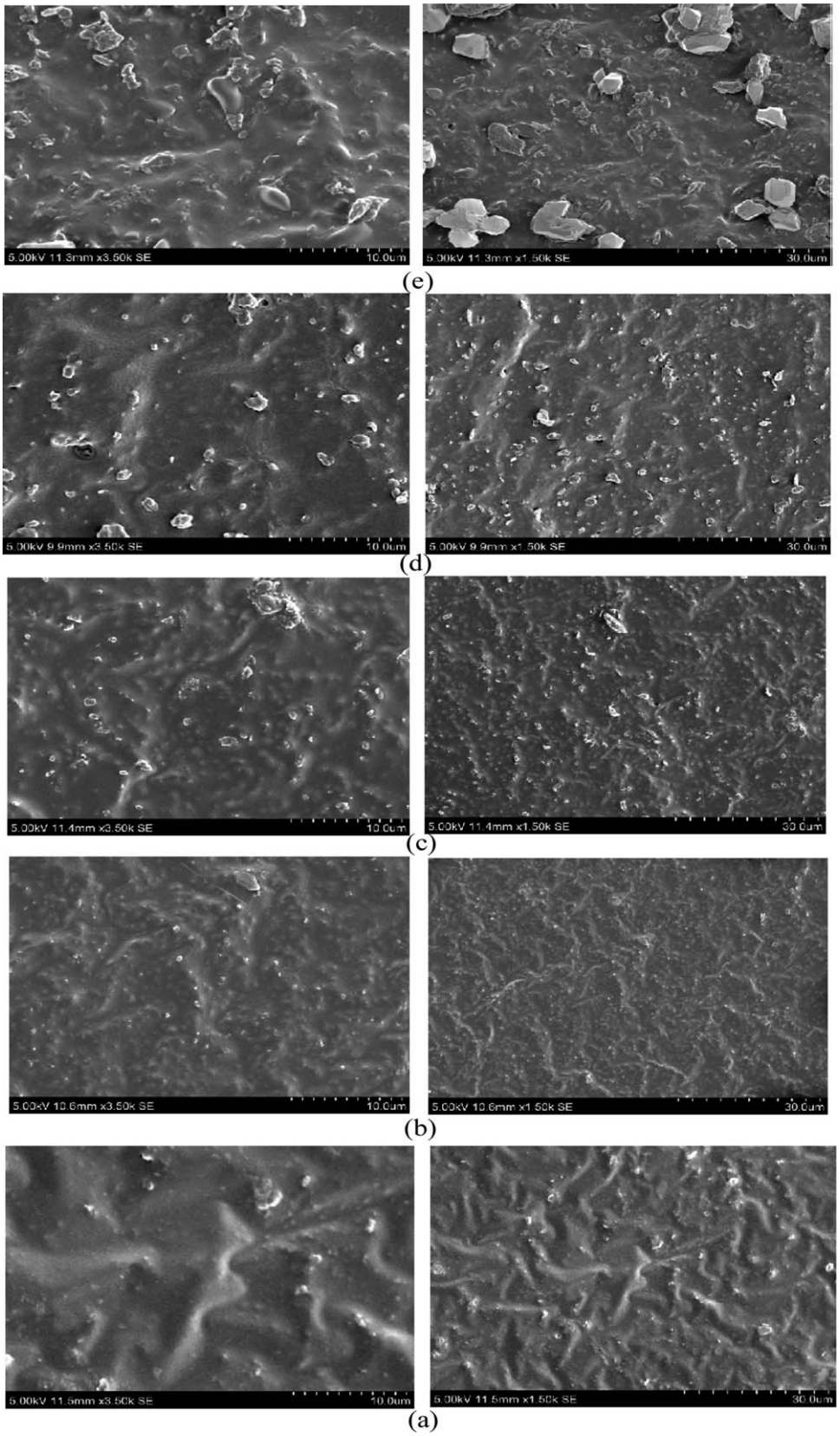

Figure 15. SEM of (a) CIIR-0, (b) CIIR-5, (c) CIIR-10, (d) CIIR-15, and (e) CIIR-20.

CONCLUSIONS

HBP-OMMT was prepared by condensation polymerization between OMMT, AB2 monomer, and the hindered phenol. It was a type of effective filler for improving the mechanical and damping properties of CIIR composites. Experimental results demonstrated that incorporation of 15 phr of HBP-OMMT into the CIIR matrix could improve the tensile strength, elongation at break, thermal stability, and damping performance of the composites. The tensile strength and elongation at break were 7.6 MPa and 1066%, respectively, which were changed about 41 and 20% compared with that of pure CIIR, 5.4 MPa and 890%. The thermal stability of CIIR-15 was also improved. $T_{5\%}$ and T_{max} were 323.3 and 410.5 °C, respectively. Moreover, the damping performance was improved effectively. Tan δ of CIIR-15 was increased from 1.20 to 1.44, while E', E'', and the effective damping temperature ranges also became wider.

The mechanism for the improved reinforcing and damping abilities of HBP-OMMT was put forward. Modification of MMT by HBP could increase the chain interactions in CIIR matrix, and thus may improve the mechanical, thermal, and damping performance of the composites. In addition, a large number of hydrogen bonds were formed in the composites and they were helpful for the improvement of above damping performance.

ACKNOWLEDGMENTS

This work was financially supported by "National Natural Science Funds (Project No.51173102)".

REFERENCES

1. Chen, S. B.; Wang, Q. H. *Mater. Chem. Phys.* **2011**, *130*, 680.
2. Ferry, J. D.; Grandine, L. D.; Fitzgerald, E. R. *J. Appl. Polym. Sci.* **1953**, *24*, 911.
3. Huang, G. S.; He, X. R.; Wu, J. R. *J. Appl. Polym. Sci.* **2006**, *102*, 3127.
4. Maria, H. J.; Lyczko, N.; Nzihou, A.; Joseph, K.; Mathew, C.; Thomas, S. *Appl. Clay Sci.* **2014**, *87*, 120.
5. Sajjayanukul, T.; Saeoui, P.; Sirisinha, C. *J. Appl. Polym. Sci.* **2005**, *97*, 2197.
6. Zhou, J. F.; Wu, J. S. *New Chem. Mater.* **2010**, *38*, 114.
7. Tiwari, S. K.; Sahoo, B. P.; Mahapatra, S. P. *Plast. Rubber Compos.* **2014**, *43*, 145.
8. Wu, J. R.; Huang, G. S.; Wang, X. A.; He, X. J.; Lei, H. X. *J. Polym. Res.* **2011**, *18*, 2213.
9. Yu, Y.; Gu, Z.; Song, G. J.; Li, P. Y.; Li, H. H.; Liu, W. S. *Appl. Clay Sci.* **2011**, *52*, 381.
10. Mohamed, R. M. *J. Ind. Eng. Chem.* **2013**, *19*, 80.
11. Qiao, B.; Zhao, X. Y.; Yue, D. M. *J. Mater. Chem.* **2012**, *22*, 1233.
12. Su, C.; He, P.; Yan, R. J. *Polym. Compos.* **2012**, *33*, 860.
13. Wu, C. F.; Yamagishi, T. A.; Nakamoto, Y.; Ishida, S.; Nitta, K. H.; Kubota, S. *J. Polym. Sci. Part B: Polym. Phys.* **2000**, *38*,
14. Wang, J. C.; Chen, Y. H.; Wang, J. H. *J. Appl. Polym. Sci.* **2009**, *111*, 658.
15. Peng, Z. J.; Wu, X. J. *Fine Chem.* **2006**, *9*, 873.
16. Kou, Y. X.; Tong, S. Y.; Liu, X. T.; Zeng, G. M.; Wen, J. S. *J. Funct. Polym.* **2005**, *2*, 305.
17. Huskić, M.; Žigon, M.; Ivanković, M. *Appl. Clay Sci.* **2013**, *85*, 109.
18. Sun, H. G.; Zhang, J. C.; Li, L.; Xu, J.; Sun, D. *Colloid Surf. A* **2013**, *426*, 26.
19. Kozak, M.; Domka, L. *J. Phys. Chem.* **2004**, *65*, 441.
20. Gao, D.; Li, R.; Lv, B.; Ma, J. Z.; Tian, F.; Zhang, J. *Compos. Part B* **2015**, *77*, 329.
21. Amin, A.; Darweesh, H. H. M.; Morsi, S. M. M.; Ayoub, M. M. H. *J. Appl. Polym. Sci.* **2011**, *120*, 3054.
22. Amin, A.; Darweesh, H. H. M.; Ramadan, A. M.; Morsi, S. M. M.; Ayoub, M. M. H. *J. Appl. Polym. Sci.* **2011**, *121*, 309.
23. Seyidoglu, T. J.; Yilmazer, U. K. *J. Thermoplast. Compos.* **2013**, *10*, 5.
24. Wang, J. C.; Sun, K.; Hao, W. L.; Du, Y. C.; Pan, C. *Appl. Clay Sci.* **2014**, *90*, 109.
25. Amin, A.; Samy, M. *Int. J. Polym. Sci.* **2013**, *2013*, 1.
26. Vaia, A. V.; Teukolsky, R. K.; Giannelis, E. P. *Chem. Mater.* **1994**, *6*, 1017.
27. Piscitelli, F.; Posocco, P.; Toth, R.; Fermeglia, M.; Pricl, S.; Mensitieri, G.; Lavorgna, M. *J. Colloid Int. Sci.* **2010**, *351*, 108.
28. Zhang, Q.; Meng, Z. L. *Water Sci. Technol.* **2014**, *69*, 1798.
29. Tiwari, R. R.; Chillier, K. C.; Natarajan, U. *Appl. Clay Sci.* **2008**, *38*, 203.
30. Mansoori, Y.; Masooleh, T. R. M. *Polym. Compos.* **2015**, *36*, 613.
31. Balek, V.; Benes, M.; Malek, Z. *J. Therm. Anal. Calorim.* **2006**, *83*, 617.
32. Hedley, C. B.; Yuan, G. *Appl. Clay. Sci.* **2007**, *35*, 180.
33. Zidelkheir, B.; Abdelgoad, M. *J. Therm. Anal. Calorim.* **2008**, *94*, 181.
34. He, H. P.; Frost, R. L.; Deng, F. *Clay. Clay Miner.* **2004**, *52*, 350.
35. Abreu, A. S.; Oliveira, M. *Carbohyd. Polym.* **2015**, *129*, 127.
36. Wang, J. C.; Yang, K.; Zheng, X. Y. *Proceedings of 2009 International Conference on Advanced Fibers and Polymer Materials* **2009**, *2*, 1019.
37. Dodiuk-Kenig, H.; Lizenboim, K. *J. Adhes. Sci. Technol.* **2004**, *18*, 1723.
38. Mo, Z. L.; Niu, G. P. *Electron. Mater. Lett.* **2008**, *62*, 1743.
39. Bourbigot, S.; Vanderhart, D.; Gilman, J.; Awad, W.; Davis, R.; Morgan, A.; Wilkie, C. *J. Polym. Sci. Part B: Polym. Phys.* **2003**, *41*, 3188.

SGML and CITI Use Only
DO NOT PRINT